ACS APPLIED MATERIALS & INTERFACES

Forum Article

www.acsami.org

Nitrogen-Doped Carbon Nanofiber/Molybdenum Disulfide Nanocomposites Derived from Bacterial Cellulose for High-Efficiency Electrocatalytic Hydrogen Evolution Reaction

Feili Lai,[†] Yue-E Miao,[*,‡] Yunpeng Huang,[†] Youfang Zhang,[†] and Tianxi Liu[*,†,‡]

[†]State Key Laboratory of Molecular Engineering of Polymers, Department of Macromolecular Science, Fudan University, Shanghai 200433, P. R. China

[‡]State Key Laboratory of Modification of Chemical Fibers and Polymer Materials, College of Materials Science and Engineering, Donghua University, Shanghai 201620, P. R. China

Supporting Information

ABSTRACT: To remit energy crisis and environmental deterioration, non-noble metal nanocomposites have attracted extensive attention, acting as a fresh kind of cost-effective electrocatalysts for hydrogen evolution reaction (HER). In this work, hierarchically organized nitrogen-doped carbon nanofiber/molybdenum disulfide (pBC-N/MoS_2) nanocomposites were successfully prepared via the combination of in situ polymerization, high-temperature carbonization process, and hydrothermal reaction. Attributing to the uniform coating of polyaniline on the surface of bacterial cellulose, the nitrogen-doped carbon nanofiber network acts as an excellent three-dimensional template for hydrothermal growth of MoS_2 nanosheets. The obtained hierarchical pBC-N/MoS_2 nanocomposites exhibit excellent electrocatalytic activity for HER with small overpotential of 108 mV, high current density of 8.7 mA cm^{-2} at η = 200 mV, low Tafel slope of 61 mV dec^{-1}, and even excellent stability. The greatly improved performance is benefiting from the highly exposed active edge sites of MoS_2 nanosheets, the intimate connection between MoS_2 nanosheets and the highly conductive nitrogen-doped carbon nanofibers and the three-dimensional networks thus formed. Therefore, this work provides a novel strategy for design and application of bacterial cellulose and MoS_2-based nanocomposites as cost-effective HER eletrocatalysts.

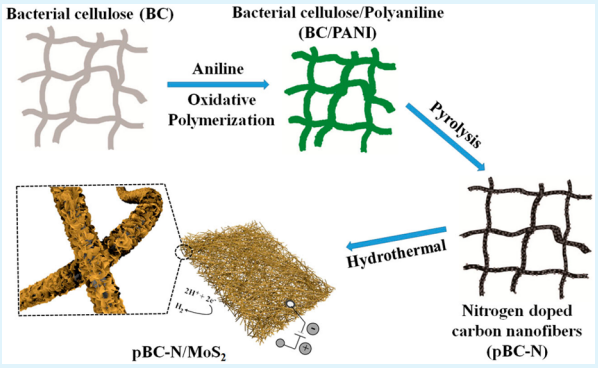

KEYWORDS: *MoS_2 nanosheets, nitrogen-doped carbon nanofibers, bacterial cellulose, polyaniline, hydrogen evolution reaction*

1. INTRODUCTION

To remit energy crisis, hydrogen is believed to be an ideal substitution for fossil fuels, because of its extraordinary characteristics of high efficiency, eco-friendliness, and cleanliness.[1,2] However, excessive burning of fossil fuels, biomass, natural gas, and coal to produce hydrogen, has given rise to substantial carbon dioxide emission being neither renewable nor carbon-neutral.[3,4] Water splitting reaction is hailed as a promising approach to produce cost-effective energy, which can be divided into two half-reactions: the oxygen evolution reaction (OER) and hydrogen evolution reaction (HER).[5−7] Hydrogen is produced from the half-reaction of HER,[8,9] which heavily depends on the highly efficient catalysts to overcome the intrinsically slow HER kinetics of semiconductors. Traditionally, platinum (Pt) based materials, such as platinum (Pt),[10] Pt/sliver,[11] and Pt/carbon catalysts,[12] have been regarded as the most effective electrocatalysts for HER, which show near-zero overpotentials under acidic conditions. In spite of the outstanding performance of platinum group metals, the scarcity and high cost of platinum have severely restricted its applications. Therefore, it is an irresistible trend to develop non-noble metal composites with high abundance and low cost as highly active HER electrocatalysts.[13,14]

MoS_2 is one of the most promising candidates due to its excellent electrocatalytic activity, chemical stability, and simple preparation process.[15−17] Lau et al. prepared MoS_2 nanoparticles in an imidazolium ionic liquid medium, which exhibited delayered morphology with large number of active edge sites.[18] Yan et al. synthesized well-defined ultrathin MoS_2 nanoplatelets via a facile solvent-dependent route by controlling the ratio of dimethylformamide and H_2O, showing a small onset potential of 0.09 V and a low Tafel slope of 53 mV dec^{-1} as HER electrocatalyst.[19] Nevertheless, severe restacking resulting from the high surface energy and van der Waals

Special Issue: Applied Materials and Interfaces in China

Received: July 13, 2015
Accepted: August 18, 2015
Published: August 24, 2015

DOI: 10.1021/acsami.5b06274
ACS Appl. Mater. Interfaces 2016, 8, 3558−3566

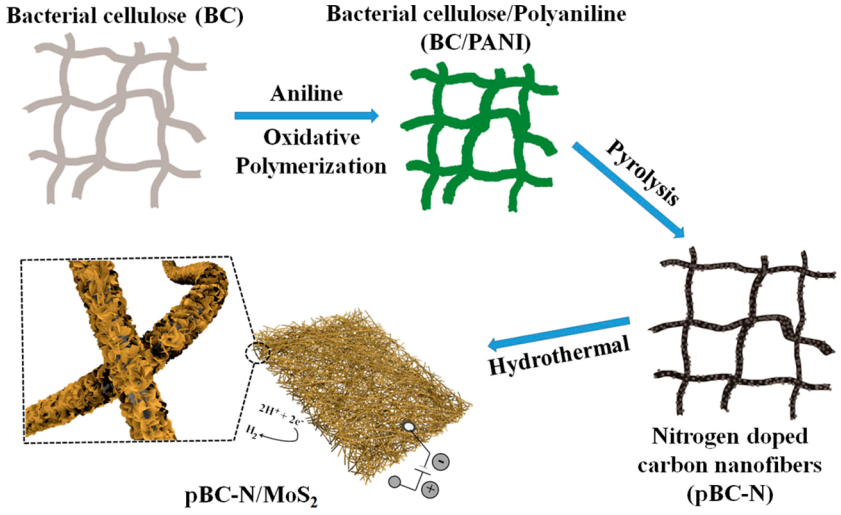

Figure 1. Schematic for the preparation of pBC-N/MoS_2 nanocomposites.

attractions between MoS_2 interlayers drastically reduces its electrocatalytic activity for HER. Therefore, it is of great necessity to construct uniformly distributed MoS_2 nanostructures for optimized electrochemical performance.

Hybridization of MoS_2 with other highly conductive materials to form hierarchical nanostructures is an effective approach to improve the dispersion of MoS_2 nanoparticles and enhance its conductivity to achieve optimal catalytic activity. Li et al. developed a selective solvothermal synthesis of MoS_2 nanoparticles on reduced graphene oxide sheets, which exhibited superior electrocatalytic activity for HER with a low overpotential of 100 mV, a small Tafel slope of 41 mV dec^{-1} and a high catalytic stability.[20] Composites of TiO_2 nanotubes coated with layered MoS_2 nanoparticles were fabricated by photocatalytic strategy showing a high electrocatalytic activity in hydrogen evolution reactions with an onset overpotential of −0.14 V and a Tafel slope of 52 mV dec^{-1}.[21] However, the harsh synthesis conditions and high cost severely limit the widespread commercialization of these electrocatalytic materials, which makes it an emergency to develop more cost-effective materials with high electrocatalytic activity.

Bacterial cellulose (BC) derived from biomass precursors via a microbial fermentation has attracted growing interest because of its abundant resource, low cost, and eco-friendliness,[22−24] being one of the most promising candidates for energy conversion and storage applications.[25−27] Moreover, the three-dimensional networks constructed by superfine bacterial cellulose nanofibers (ca. 50 nm in diameter) can dramatically enhance the specific surface area and be beneficial to excellent electrolyte wettability and fast ion penetration. Furthermore, introduction of heteroatoms (e.g., nitrogen or phosphorus) into carbonaceous materials can adjust the valence orbital energy levels of the adjacent carbon atoms in carbon nanofibers to induce synergistically enhanced electrocatalytic property.[28] Liang et al. prepared a highly active nitrogen-doped carbon nanofiber aerogel as metal-free electrocatalyst, showing superior activity, high selectivity and excellent electrochemical stability for oxygen reduction reactions.[29] Similarly, nitrogen-doped porous graphene materials also showed remarkable electrocatalytic properties toward HER, because of the existence of nitrogen atoms.[28] Therefore, nitrogen doping is verified as one of the most promising methods to enhance the electrocatalytic activity of electrode materials.

Herein, cost-effective electrocatalyst of nitrogen-doped carbon nanofiber/MoS_2 (pBC-N/MoS_2) nanocomposites was prepared through the combination of oxidative polymerization of aniline on the surface of bacterial cellulose nanofibers, high-temperature carbonization process and hydrothermal growth of MoS_2 nanosheets. The obtained pBC-N/MoS_2 nanocomposites with hierarchical nanostructures show excellent electrocatalytic activity toward HER with small overpotential of 108 mV, high current density of 8.7 mA cm^{-2} at η = 200 mV and excellent stability, which is related to the highly conductive nitrogen-doped carbon nanofibers, homogeneously distributed MoS_2 nanosheets with highly exposed active edge sites, and the synergistic effect between nitrogen atom and MoS_2. Hence, it is a promising approach to construct hybrid nanostructures of bacterial cellulose and MoS_2 as the next-generation electrocatalysts for hydrogen evolution reaction.

2. MATERIALS AND METHODS

Materials. The bacterial cellulose pellicles (30 × 40 cm^2) were purchased from Hainan Yide Food Co. Ltd. Hexaammonium heptamolybdate tetrahydrate [$(NH_4)_6Mo_7O_{24}{\cdot}4H_2O$], aniline (ANI), ammonium persulfate [$(NH_4)_2S_2O_8$, APS], sodium hydroxide (NaOH), hydrochloricacid (HCl) and dimethylformamide (DMF) were all purchased from Sinopharm Chemical Reagent Co. Thiourea (CH_4N_2S) was purchased from Aladdin Chemical Reagent Co. All chemicals were of analytic grade and used without further purification.

Preparation of pBC-N Nanofibers. The BC pellicles in rectangular squares (4 × 5 cm^2) were immersed into 0.1 M NaOH solution for 6h, and then washed by deionized water for several times to neutral. Then, the rectangular BC pellicles were frozen in liquid nitrogen (−196 °C), and subsequently freeze-dried. The as-obtained BC (100 mg) was immersed into 75 mL HCl solution (1 mol L^{-1}) containing varied molar concentrations (0.004, 0.04 and 0.4 M) of aniline monomers for 24 h under vigorous stirring, to ensure the sufficient adsorption of aniline hydrochloride solution into the networks of bacterial cellulose via hydrogen bonding, after which it was placed into an ice−water bath. Kept at 0 °C, another 75 mL of HCl solution (1 mol L^{-1}) dissolving different amounts (34.2, 342 and 3420 mg, respectively) of APS was added dropwise into the above solution in 30 min and reacted for 5 h to ensure the full polymerization of aniline monomers into polyaniline (PANI). Then, the obtained materials (named as BC/PANI) were washed with deionized water for several times to remove the excessive PANI on the surface of BC and freeze-dried for 24 h. Finally, BC/PANI hybrid membranes were pyrolyzed under an Ar atmosphere at 800 °C for 2 h

DOI: 10.1021/acsami.5b06274
ACS Appl. Mater. Interfaces 2016, 8, 3558−3566

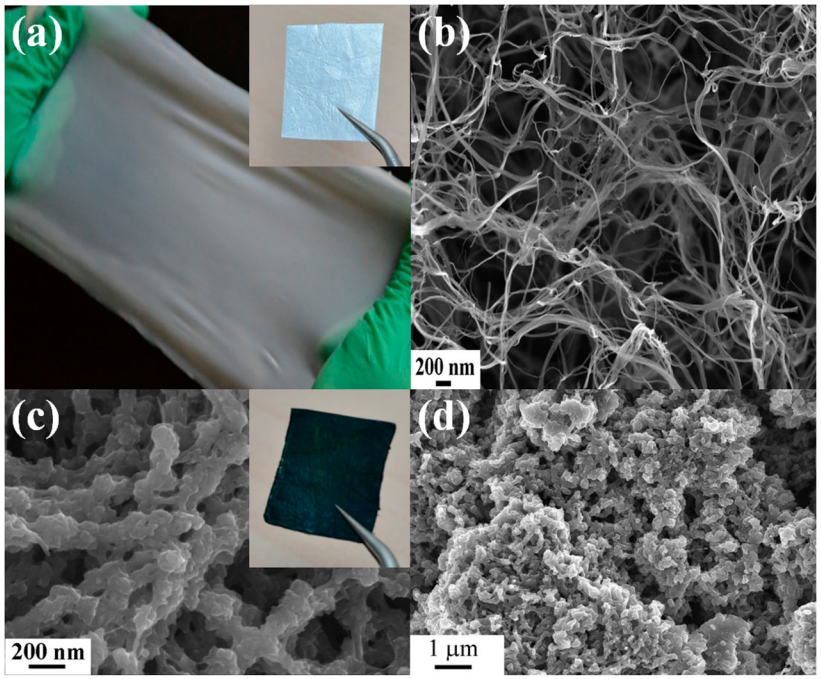

Figure 2. (a) Photograph of the pristine BC pellicle and freeze-dried BC membrane (inset); (b) FESEM image of pBC nanofibers; (c) FESEM image of pBC-N2 nanofibers and photograph of BC/PANI hybrid membrane (inset); (d) FESEM image of pure PANI powder.

with a heating rate of 5 °C min^{-1}. The generated black materials were respectively denoted as pBC-N1, pBC-N2, and pBC-N3 with the increase in ANI amount. Additionally, the BC pellicle was directly pyrolyzed via the same temperature-rising program to obtain pBC.

Preparation of pBC-N/MoS_2 Nanocomposites. Typically, 20 mg of powdery pBC-N2 nanofibers were added into 25 mL of homogeneous composite solution of $(NH_4)_6Mo_7O_{24}{\cdot}4H_2O$/thiourea with the mole ratio of 1:2. Subsequently, the resulting mixture was transferred to a Teflon-lined autoclave and hydrothermally treated at 200 °C for 24 h. Then, the obtained products were washed with distilled water, and overnight dried at 70 °C in air, which were respectively named as pBC-N2/MoS_2-10, pBC-N2/MoS_2-90, pBC-N2/MoS_2-180, and pBC-N2/MoS_2-360 corresponding to the different amounts (10, 90, 180, and 360 mg) of $(NH_4)_6Mo_7O_{24}{\cdot}4H_2O$. In addition, pure MoS_2 powder and pBC/MoS_2-90 were prepared by the same step for comparison. The overall preparation procedure of pBC-N/MoS_2 nanocomposites was schematically shown in Figure 1.

Characterization. Morphologies of the samples (coated with a thin layer of gold prior to observations) were investigated by field-emission scanning electron microscope (FESEM, Ultra 55, Zeiss) at an acceleration voltage of 5 kV. Transmission electron microscopy (TEM) images were performed on a JEOL-2010 transmission electron microscope at an acceleration voltage of 200 kV. The specific surface area was calculated by the conventional Brunauer–Emmet–Teller (BET) method with a belsorp-max surface area detecting instrument (Tristar3000). The pore size distribution was derived from the adsorption branches of isotherms by Barrett–Joyner–Halenda (BJH) method. Phases of the samples were conducted by X-ray diffraction (XRD, X'pert PRO, PANalytical) with Cu K_α radiation (λ = 0.1542 nm) at a speed of 5° min^{-1} from 2θ = 10 to 80° under a voltage of 40 kV and a current of 40 mA. X-ray photoelectron spectroscopy (XPS) analyses of the chemical composition were carried out on a RBD upgraded PHI-5000C ESCA system (PerkinElmer) with Mg K_α radiation ($h\nu$ = 1253.6 eV). All XPS spectra were corrected using C 1s line at 284.6 eV while the curve fitting and background subtraction were accomplished using RBD AugerScan 3.21 software.Thermogravimetric analysis (Pyris 1 TGA, PerkinElmer) was performed in air from 100 to 700 °C at a heating rate of 20 °C min^{-1} to measure the mass content of MoS_2 in the nanocomposites.

Electrochemical Measurements. Prior to all electrochemical measurements, the glassy carbon electrodes (GCE) were successively polished with 1.0, 0.3, and 0.05 μm alumina slurries, sonicated in alcoholic solution for 15 min, and dried at room temperature in a desiccator. Afterward, 2 mg of pBC-N2/MoS_2, pBC-N2 nanofibers or pBC was dispersed in 1 mL of a mixed solution of DMF/distilled water (v/v, 1:1) containing 50 μL Nafion solution (5% Nafion in ethanol). Then, 15 μL of the above solution was dropped onto GCE and dried at room temperature to yield pBC-N2/MoS_2, pBC-N2 or pBC-modified GCE.

Electrochemical measurements were performed on a CHI 660D electrochemical workstation (Shanghai Chenhua Instrument Co., China) at room temperature. In a standard three-electrode, GCEs modified with different catalysts were used as the working electrodes, Pt wire as the counter electrode, and saturated calomel electrode (Hg/$HgCl_2$ in saturated KCl, SCE) as the reference electrode, respectively. The electrocatalytic activity of the nanocomposites toward reversible hydrogen electrode (RHE) was examined using liner sweep voltammetry (LSV) in nitrogen-purged 0.5 M H_2SO_4 at a scan rate of 2 mV s^{-1}. All the potentials reported in this work were calibrated to RHE according to the equation of $E_{RHE} = E_{SCE} + (0.241 + 0.059\ pH)$ V. The long-term potential cycling stability of pBC-N2/MoS_2-90 nanocomposite was conducted in the potential ranging from −0.4 to 0.2 V for 1000 cycles at an accelerated scanning rate of 100 mV s^{-1}. Electrochemical impedance spectroscopy (EIS) measurements were conducted in 0.5 M H_2SO_4 by applying an AC voltage in the frequency range between 100 kHz and 10 mHz with 5 mV amplitude.

3. RESULTS AND DISCUSSION

Derived from freeze-dried original BC pellicles (Figure 2a), spumescent BC aerogel with 3 mm in thickness (inset in Figure 2a) is obtained, providing a three-dimensional network with interconnected pores. After the pyrolytic process of BC aerogel, superfine carbon nanofibers with diameter of 30–60 nm (Figure 2b) were formed. As reported in previous works, the rich hydroxyl groups of BC aerogel could interact with amine groups of aniline through hydrogen bonding, thus contributing to the uniform in situ polymerization of aniline inside the network of BC.[30] Then, BC/PANI hybrid membranes (inset in

DOI: 10.1021/acsami.5b06274
ACS Appl. Mater. Interfaces 2016, 8, 3558–3566

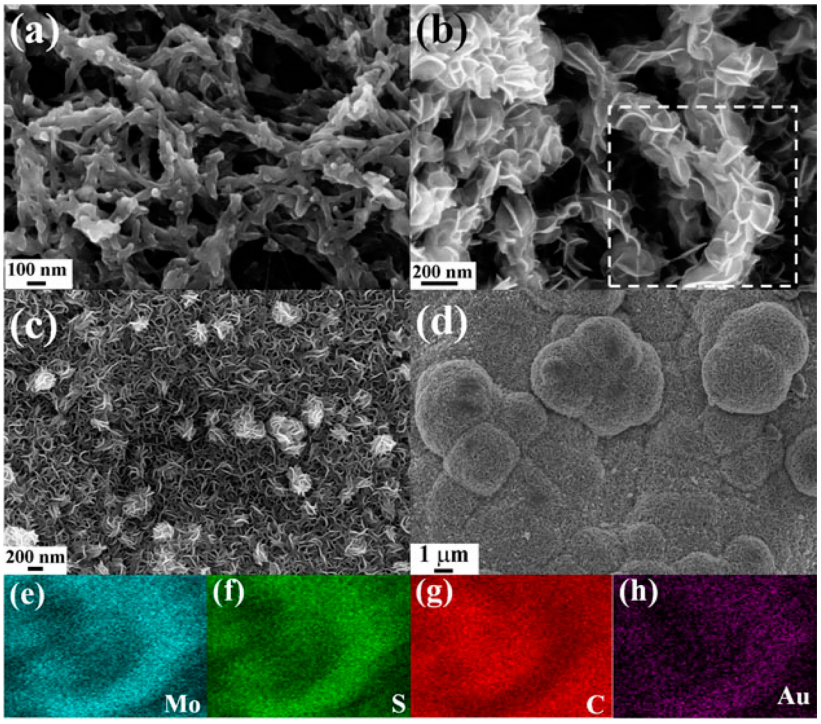

Figure 3. FESEM images of (a) pBC-N2/MoS_2-10, (b) pBC-N2/MoS_2-90, (c) pBC-N2/MoS_2-180, (d) pBC-N2/MoS_2-360 nanocomposites. The corresponding EDS elemental mappings of pBC-N2/MoS_2-90 nanocomposite: (e) Mo, (f) S, (g) C, and (h) Au.

Figure 2c) were pyrolyzed at 800 °C to successfully form core−shell pBC-N2 nanofibers (Figure 2c) with diameter of ca. 200 nm, which can efficiently prevent the serious aggregation of PANI particles (Figure 2d). Because of the limited and overexcessive growth of PANI on the surface of BC nanofibers, the obtained pBC-N1 (Figure S1a) and pBC-N3 ((Figure S1b) nanofibers are neither suitable to be the templates for further growth of MoS_2 nanosheets. Moreover, the coarse surface of N-doped carbon nanofibers and thus formed three-dimensional porous network structures are beneficial to the diffusion of MoS_2 precursors into the inner space and in situ reduction into MoS_2 nanosheets on the surface of nanofibers. Therefore, pBC-N2 nanofiber is considered as an optimal template for further growth of MoS_2 nanosheets.

With different mass ratios of MoS_2 precursor to pBC, pBC-N2/MoS_2 nanocomposites are prepared. As shown in Figure 3a, only sparse MoS_2 nanparticles are interspersed on the surface of pBC-N2 for pBC-N2/MoS_2-10 nanocomposite. When the loading mass of $(NH_4)_6Mo_7O_{24}{\cdot}4H_2O$ is increased to 90 mg, ultrathin MoS_2 nanosheets are uniformly anchored on the surface of carbon nanofibers to form pBC-N2/MoS_2-90 nanocomposite (Figure 3b), which can significantly improve the dispersion of MoS_2 nanosheets (Figure S2). The corresponding energy-dispersive spectra (EDS) shown in Figure 3e−h display the elemental distribution of Mo, S, and C, indicating the successful growth of MoS_2 on the surface of carbon nanofibers. The morphology of pBC-N2/MoS_2-90 nanocomposite is further confirmed by TEM observations, showing an overall diameter of about 600 nm (Figure S3a). Furthermore, the magnified image in Figure S3b also indicates the good connection between MoS_2 nanosheets and the nitrogen-doped carbon nanofiber template. With further increasing the dosage of $(NH_4)_6Mo_7O_{24}{\cdot}4H_2O$, pBC-N2 nanofibers are totally covered with densely packed MoS_2 nanosheets (Figure 3c). For pBC-N2/MoS_2-360 nanocomposite, micrometer-sized balls consisting of MoS_2 nanosheets vastly aggregate even on the surface of the three-dimensional carbon nanofiber networks, due to the limited space of pBC-N2 template for further distribution of MoS_2 nanosheets. Brunauer−Emmett−Teller (BET) analysis further reveals a high specific surface area of 188.1 $m^2\ g^{-1}$ for pBC-N2/MoS_2-90 nanocomposite with the pore size distribution in the range of 5 to 20 nm as illustrated in Figure 4, indicating sufficient

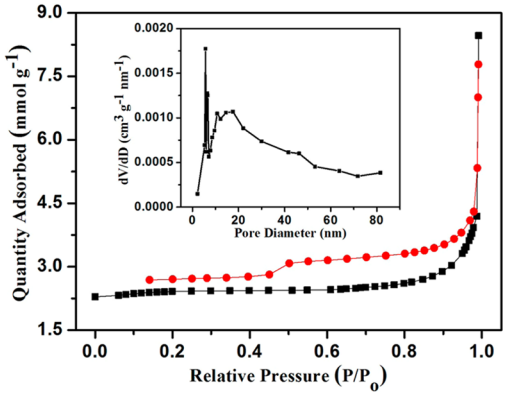

Figure 4. N_2 adsorption/desorption isotherm and the corresponding pore size distribution (inset) of pBC-N2/MoS_2-90 nanocomposite.

mesopores for effective electrochemical activation of MoS_2 nanosheets. Therefore, pBC-N2/MoS_2-90 nanocomposite with MoS_2 nanosheets more uniformly and densely anchored on the surface of nitrogen-doped carbon nanofibers not only maintains the three-dimensional structure of bacterial cellulose for fast penetration of ions into the inner space but also provides plenty of active sites for rapid electrochemical reactions.

DOI: 10.1021/acsami.5b06274
ACS Appl. Mater. Interfaces 2016, 8, 3558−3566

Structural features of the resultant samples were revealed by XRD patterns. Three sharp peaks centered at 2θ = 15.1, 17.5, and 23.5° for both freeze-dried BC and BC/PANI hybrid membranes (Figure S4) are assigned to $(1\bar{1}0)$, (110) and (220) planes of bacterial cellulose as reported previously.[31] Pure PANI is amorphous with two broad peaks centered at 2θ = 20.5 and 25.8°, which are ascribed to the periodicity parallel and perpendicular to PANI chains, respectively.[32] Three distinct diffraction peaks at 2θ = 14.9, 33.0, and 58.1° of pBC-N2/MoS_2 nanocomposite (Figure 5) can be successfully indexed to (002), (100), and (110) reflections of MoS_2, respectively.[33] To be emphasized, the XRD pattern of pBC-N2/MoS_2-10 nanocomposite is close to that of pBC-N2 with broad diffraction peaks of typical amorphous carbon instead of MoS_2, which is caused by the sparsely interspersed MoS_2 nanoparticles on the surface of pBC-N2 nanofibers as shown in Figure 3a. Further insights into the surface information on the nanocomposites are obtained from XPS spectra, as shown in Figure 6. The XPS survey spectrum of pBC-N2/MoS_2-90 nanocomposite (Figure 6a) clearly reveals the incorporation of nitrogen atoms within carbon nanofibers. Moreover, the high-resolution N 1s spectrum (Figure 6b) is well-fitted into three peaks centered at 398.0, 399.8, and 401.1 eV, corresponding to the pyridinic-like, pyrrolic-like, and graphitic nitrogen, respectively. Figure 6c, d depicts the high-resolution scans of Mo 3d and S 2p spectra. The characteristic peaks of Mo^{4+} located at 228.2 and 232.1 eV, and S^{2-} located at 161.5, 162.7, and 225.9 eV, further signify the formation of MoS_2 on the surface of pBC-N2 nanofibers.[34] As shown in Figure S5, the weight loss of 98 and 13% is respectively observed for pure pBC-N2 and MoS_2 nanoparticles after they are heated up over 700 °C, indicating the complete decomposition of the pBC-N2 template and successful transformation of MoS_2 to molybdenum oxide and SO_2 in air. Therefore, the weight loss for pBC-N2/MoS_2 nanocomposites covers not only the oxidation reaction of MoS_2 nanosheets but also the complete decomposition of the pBC-N2 template. So, the loading amounts of MoS_2 can be calculated from TGA curves, being 6.3, 21.1, 58.3, and 84.0% for pBC-N2/MoS_2-10, pBC-N2/MoS_2-90, pBC-N2/MoS_2-180, and pBC-N2/MoS_2-360 nanocomposites, respectively.

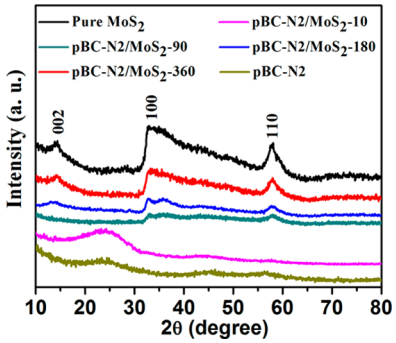

Figure 5. XRD patterns of pure MoS_2 powder and pBC-N2/MoS_2-10, pBC-N2/MoS_2-90, pBC-N2/MoS_2-180, pBC-N2/MoS_2-360, and pBC-N2 nanocomposites.

HER measurements are carried out in 0.5 M H_2SO_4 solution with a three-electrode configuration at a scan rate of 2 mV s^{-1}. Figure 7a shows the $j-V$ plots of pBC-N2, pBC-N2/MoS_2-10, pBC-N2/MoS_2-90, pBC-N2/MoS_2-180, pBC-N2/MoS_2-360, and commercial Pt/C (Johnson Matthey, Hispec 3000, 20 wt %) modified GCE, respectively. It can be seen that pBC-N2 modified GCE exhibits negligible current flow in the potential range from −300 to 0 mV, which is consistent with the previous works on nitrogen-doped carbon materials.[28] On the contrary, pBC-N2/MoS_2-90 modified GCE exhibits apparent cathodic currents at the negative potential of −0.108 V (vs RHE), with higher current densities of 2.1 and 8.7 mA cm^{-2} at overpotentials (η) of 150 and 200 mV, respectively. This low overpotential of 108 mV, approaching the near zero over-

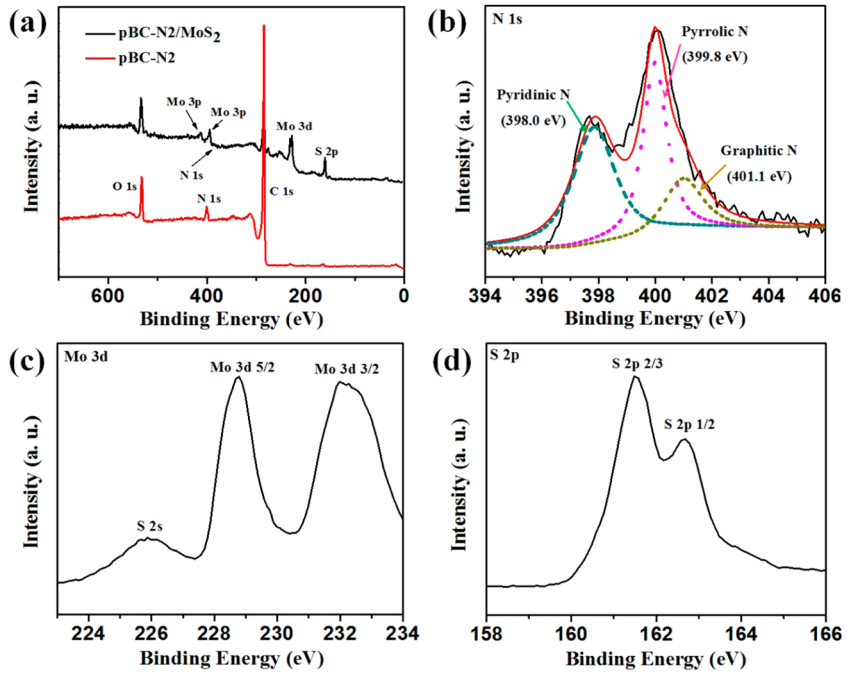

Figure 6. (a) XPS survey spectra of pBC-N2 and pBC-N2/MoS_2-90 nanocomposites; (b) high-resolution N 1s XPS spectrum of pBC-N2 nanofibers. High-resolution XPS spectra of pBC-N2/MoS_2-90 nanocomposite: (c) Mo 3d and (d) S 2p.

DOI: 10.1021/acsami.5b06274
ACS Appl. Mater. Interfaces 2016, 8, 3558−3566

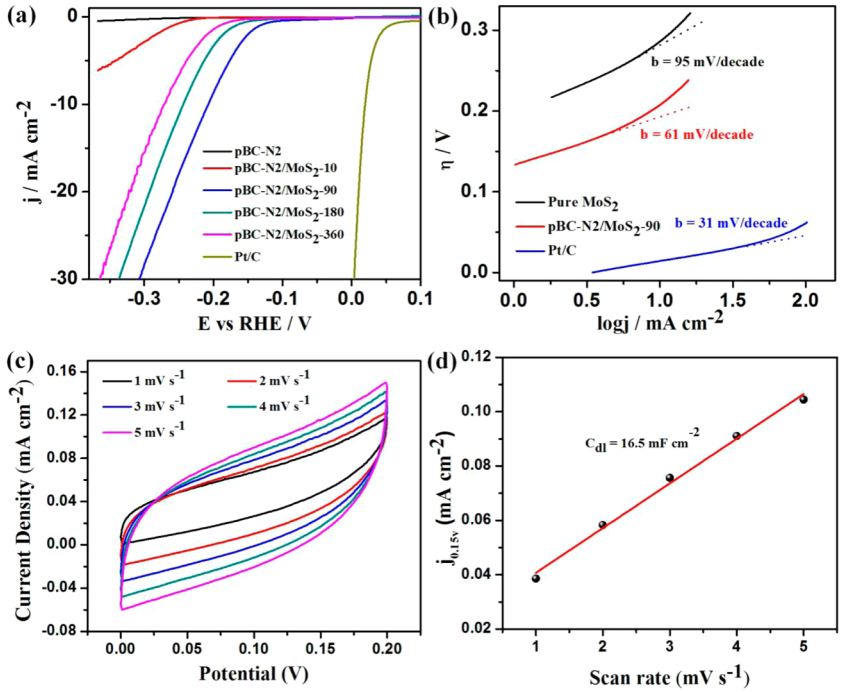

Figure 7. (a) Polarization curves of pBC-N2, pBC-N2/MoS_2 and Pt/C modified GCE in 0.5 M N_2-purged H_2SO_4 solution; (b) Tafel plots of pure MoS_2, pBC-N2/MoS_2-90, and Pt/C modified GCE derived from the polarization curves; (c) Voltammograms of pBC-N2/MoS_2-90 modified GCE at various scan rates; (d) Linear fitting for the capacitive currents of the catalyst vs scan rates.

potential of Pt/C modified GCE, is superior over the results reported previously (Table S1), such as commercial bulk MoS_2 (350 mV),[35] defect-rich MoS_2 nanosheets (120 mV),[36] and MoS_2/TCNQ/carbon cloth (~120 mV),[37] indicating its high HER activity. Especially, compared with MoS_2 nanoparticles grown on carbon fiber foam derived from BC,[38] more uniform distribution of two-dimensional MoS_2 nanosheets is achieved on the surface of nitrogen-doped carbon nanofibers in our work, which successfully builds up a three-dimensional open structure for effective contact area between MoS_2 nanoparticles and electrolyte, thus leading to more negative overpotential and high current density. Meanwhile, nitrogen doping on carbon nanofibers has been proved to be a cost-efficient method to prepare non-noble metal catalyst for HER, which not only acts as "bridge" between MoS_2 nanosheets and carbon nanofibers for accelerated electron transport rate, but also as active materials for electrocatalytic reactions. As shown in Figure S6, the overpotential of pBC-N2/MoS_2-90 is superior to pBC/MoS_2-90, as nitrogen-groups can polarize the carbon atoms, induce stronger affinities toward H atoms, and consequently increase the binding energy between nitrogen doped carbon nanofibers and H atoms.[28,39,40] Moreover, pBC-N2/MoS_2 nanocomposites with different uploading masses of MoS_2 exhibit quite different catalytic activity, which is mainly decided by the effectively exposed active edge sites of MoS_2 nanosheets. The sparse growth of MoS_2 nanoparticles for pBC-N2/MoS_2-10 nanocomposite (Figure 3a) dramatically hinders HER activities, because of its scattered and discontinuous active sites on the surface of pBC-N2 nanofibers. Meanwhile, the clogged networks of pBC-N2/MoS_2-180 and pBC-N2/MoS_2-360 nanocomposites (Figure 3c, d) resulted from the excessive coverage of MoS_2 nanosheets severely impede ion penetration during the electrochemical processes, leading to confined hydrogen evolution reactions. Therefore, the porous three-dimensional networks of pBC-N/MoS_2-90 nanocomposite derived from the uniformly and immensely distributed MoS_2 nanosheets on the surface of pBC-N2 nanofibers are beneficial to fast ion penetration and electron transport, thus leading to the most excellent HER activities.

Tafel plots derived from the polarization curves of pBC-N/MoS_2-90, pBC-N, and Pt/C modified GCE are fitted well with the Tafel equation [$\eta = b \log(j) + a$, where η is the overpotential, j is the current density, and b is the Tafel slope] at different overpotential ranges, as shown in Figure 7b. The Tafel slope of pBC-N2/MoS_2-90 nanocomposite is 61 mV dec^{-1}, which is superior to that (95 mV dec^{-1}) of pure MoS_2 due to the homogeneous dispersion of MoS_2 nanosheets on the surface of highly conductive nitrogen-doped carbon nanofibers and thus generated synergistic effect between MoS_2 nanosheets and nitrogen-doped carbon nanofibers. The low Tafel slope demonstrates that pBC-N2/MoS_2-90 nanocomposite possesses a superior catalytic performance, which is comparable or superior to previous works on MoS_2 based hybrid materials.[41,42] According to the classic mechanism for HER, there are three possible reaction steps in acidic solutions.[43]

Discharge reaction (Volmer reaction):

$$H_3O^+ + e^- \rightarrow H_{ads} + H_2O \ (b \approx 120 \text{ mV dec}^{-1}) \quad (1)$$

Electrochemical desorption reaction (Heyrovsky reaction):

$$H_{ads} + H^+ + e^- \rightarrow H_2 \ (b \approx 40 \text{ mV dec}^{-1}) \quad (2)$$

Recombination reaction (Tafel reaction):

$$H_{ads} + H_{ads} \rightarrow H_2 \ (b \approx 30 \text{ mV dec}^{-1}) \quad (3)$$

Notably, the Volmer reaction should be the rate determination step for pure MoS_2 (b = 95 mV dec^{-1}) because of its serious aggregation and poor conductivity. Therefore, the dramatically reduced slope for pBC-N2/MoS_2-90 nanocomposite in the current work is attributed to the promoted Volmer

DOI: 10.1021/acsami.5b06274
ACS Appl. Mater. Interfaces 2016, 8, 3558−3566

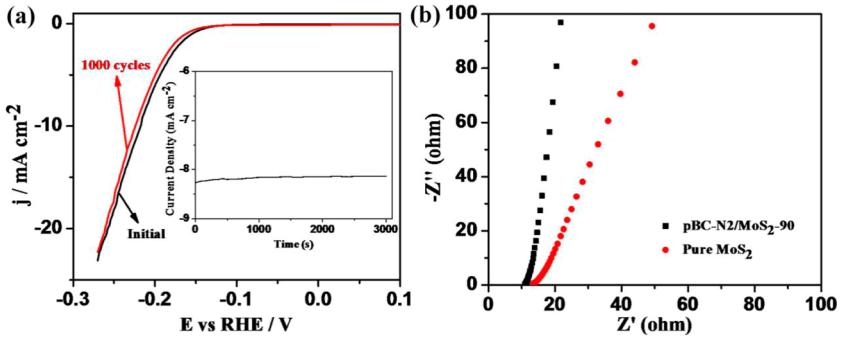

Figure 8. (a) HER polarization curves before and after 1000 cycles for pBC-N2/MoS_2-90 nanocomposite modified GCE, with the inset showing the $I-t$ curve obtained under a static overpotential of 200 mV; (b) AC impedance spectroscopy in 0.5 M H_2SO_4 from 1×10^{-2} to 1×10^{6} Hz with an AC amplitude of 5 mV.

reaction 1 rate, followed by either a Heyrovsky reaction 2 or a Tafel reaction 3, which largely results from the highly exposed active edge sites of MoS_2, uniformly distributed MoS_2 nanosheets on highly conductive carbon nanofibers, and accelerated pathways for electron transport from carbon nanofibers to catalytically active sites due to the doping of nitrogen heteroatoms. The effective surface area of pBC-N2/MoS_2-90 nanocomposite during the HER process is further determined by the double layer capacitances (C_{dl}) in the CV curves. As shown in Figure 7c, the current response in the potential window from 0 to 0.2 V (vs RHE) at different scan rates can be attributed to the double-layer charging. Thus, the C_{dl} of pBC-N2/MoS_2-90 nanocomposite is extracted by plotting the Δj at a given potential of 0.15 V (vs RHE) against the scan rate, achieving a high electrochemically effective surface area of 16.5 mF cm^{-2}. This value is higher than those of the previously reported results, such as Cu-MoS_2/rGO hybrid catalyst (15 mF cm^{-2}),[44] and $CoSe_2$ nanoparticles/carbon fiber paper catalyst (14.1 mF cm^{-2}).[16]

Stability of the obtained electrode materials in acidic environment is another important criterion for an excellent electrocatalyst. It shows similar $j-V$ curves with negligible decrease of cationic current (Figure 8a) before and after cycling tests, indicating good durability for pBC-N2/MoS_2-90 nanocomposite. It is substantially attributed to the strong chemical and electronic coupling between nitrogen-doped carbon nanofibers and MoS_2 nanosheets. The chronoamperometric measurement on pBC-N2/MoS_2-90 nanocomposite exhibits cathodic current attenuation of less than 5% within 3000 s (inset in Figure 8a), further confirms its long-term stability. EIS measurements are obtained to get insight into the HER process of pBC-N2/MoS_2 nanocomposites, which reveal lower resistance of pBC-N2/MoS_2-90 nanocomposite compared to pure MoS_2 nanoparticles. As shown in Figure 8b, no evident semicircle corresponding to the charge transfer resistance is observed for pBC-N2/MoS_2-90 nanocomposite compared with pure MoS_2 nanoparticles. In addition, the vertical slope of the linear part in the low frequency region further indicates the low diffusion resistance of ion and electron transfer for pBC-N2/MoS_2-90 nanocomposite. The apparently enhanced electrocatalytic activity benefits from the low-resistance Ohimic contact between MoS_2 nanosheets and the highly conductive nitrogen-doped carbon nanofibers,[45] largely facilitating fast ion penetration and electron transport between both MoS_2 nanosheets and nitrogen-doped carbon nanofiber networks.

4. CONCLUSIONS

In summary, nitrogen-doped carbon nanofiber/molybdenum disulfide nanocomposites with hierarchical nanostructures were successfully prepared via the combination of oxidative polymerization and hydrothermal reactions. The obtained pBC-N/MoS_2 nanocomposites exhibit excellent electrocatalytic activity as cost-effective HER electrocatalysts with small overpotential of 108 mV, high current density of 8.7 mA cm^{-2} at η = 200 mV and excellent stability, which can be attributed to the synergistic effects between nitrogen-doped carbon nanofibers and MoS_2 nanosheets for accelerated electron transport, the three-dimensional nanofiber networks for sufficient ion penetration and the highly exposed active edge sites of MoS_2 for efficient electrocatalytic reactions. Therefore, this work provides a new strategy for applying earth-abundant and cost-effective materials in energy conversion and storage areas.

■ ASSOCIATED CONTENT

Supporting Information

The Supporting Information is available free of charge on the ACS Publications website at DOI: 10.1021/acsami.5b06274.

FESEM images, TEM images, XRD patterns, TGA profiles, and polarization curves of different samples (PDF)

■ AUTHOR INFORMATION

Corresponding Authors

*E-mail: 12110440023@fudan.edu.cn.

* E-mail: txliu@fudan.edu.cn. Tel: +86-21-55664197. Fax: +86-21-65640293.

Notes

The authors declare no competing financial interest.

■ ACKNOWLEDGMENTS

The authors are grateful for the financial support from the National Natural Science Foundation of China (51125011, 51373037, 51433001).

■ REFERENCES

(1) Chu, S.; Majumdar, A. Opportunities and Challenges for a Sustainable Energy Future. *Nature* **2012**, *488*, 294−303.

(2) Candelaria, S. L.; Shao, Y.; Zhou, W.; Xiao, J.; Zhang, J. G.; Wang, Y.; Liu, J.; Li, J. H.; Cao, G. Z. Nanostructured Carbon for Energy Storage and Conversion. *Nano Energy* **2012**, *1*, 195−220.

(3) Subbaraman, R.; Tripkovic, D.; Strmcnik, D.; Chang, K. C.; Uchimura, M.; Paulikas, A.; Stamenkovic, V.; Markovic, N. Enhancing

DOI: 10.1021/acsami.5b06274
ACS Appl. Mater. Interfaces 2016, 8, 3558−3566

Hydrogen Evolution Activity in Water Splitting by Tailoring Li^+-$Ni(OH)_2$-Pt Interfaces. *Science* **2011**, *334*, 1256−1260.
(4) Cao, X.; Han, Y.; Gao, C.; Xu, Y.; Huang, X. M.; Willander, M.; Wang, N. Highly Catalytic Active PtNiCu Nanochains for Hydrogen Evolution Reaction. *Nano Energy* **2014**, *9*, 301−308.
(5) Kibsgaard, J.; Chen, Z.; Reinecke, B. N.; Jaramillo, T. Engineering the Surface Structure of MoS_2 to Preferentially Expose Active Edge Sites for Electrocatalysis. *Nat. Mater.* **2012**, *11*, 963−969.
(6) Mallouk, T. E. Water Electrolysis Divide and Conquer. *Nat. Chem.* **2013**, *5*, 362−363.
(7) He, C.; Shen, P. K. Pt Loaded on Truncated Hexagonal Pyramid WC/Graphene for Oxygen Reduction Reaction. *Nano Energy* **2014**, *8*, 52−61.
(8) Crabtree, G. W.; Dresselhaus, M. S.; Buchanan, M. V. The Hydrogen Economy. *Phys. Today* **2004**, *57*, 39−44.
(9) Hinnemann, B.; Moses, P. G.; Bonde, J.; Jorgensen, K. P.; Nielsen, J. H.; Horch, S.; Chorkendorff, I.; Norskov, J. K. Biornimetic Hydrogen Evolution: MoS_2 Nanoparticles as Catalyst for Hydrogen Evolution. *J. Am. Chem. Soc.* **2005**, *127*, 5308−5309.
(10) Szklarczyk, M.; Bockris, J. O. Photoelectrocatalysison Silicon in Solar Light. *Appl. Phys. Lett.* **1983**, *42*, 1035−1036.
(11) Bockris, J. O.; Ammar, I. A.; Huq, A. The Mechanism of the Hydrogen Evolution Reaction on Platinum Silver and Tungsten Surfaces in Acid Solution. *J. Phys. Chem.* **1957**, *61*, 879−886.
(12) Shinagawa, T.; Garcia-Esparza, A. T.; Takanabe, K. Mechanistic Switching by Hydronium Ion Activity for Hydrogen Evolution and Oxidation over Polycrystalline Platinum Disk and Platinum/Carbon Electrodes. *ChemElectroChem* **2014**, *1*, 1497−1507.
(13) Huang, Z.; Chen, Z.; Chen, Z.; Lv, C. C.; Humphrey, M.; Zhang, C. Cobalt Phosphide Nanorods as an Efficient Electrocatalyst for the Hydrogen Evolution Reaction. *Nano Energy* **2014**, *9*, 373−382.
(14) Kong, D.; Wang, H.; Lu, Z.; Cui, Y. $CoSe_2$ Nanoparticles Grown on Carbon Fiber Paper: An Efficient and Stable Electrocatalyst for Hydrogen Evolution Reaction. *J. Am. Chem. Soc.* **2014**, *136*, 4897−4900.
(15) Xu, X.; Fan, Z. Y.; Yu, X. Y.; Ding, S. J.; Yu, D. M.; Lou, X. W. A Nanosheets-on-Channel Architecture Constructed from MoS_2 and CMK-3 for High-Capacity and Long-Cycle-Life Lithium Storage. *Adv. Energy Mater.* **2014**, *4*, 1400902.
(16) Xie, J.; Zhang, J.; Li, S.; Grote, F.; Zhang, X. D.; Zhang, H.; Wang, R. X.; Lei, Y.; Pan, B. C.; Xie, Y. Controllable Disorder Engineering in Oxygen-Incorporated MoS_2 Ultrathin Nanosheets for Efficient Hydrogen Evolution. *J. Am. Chem. Soc.* **2013**, *135*, 17881−17888.
(17) Xu, X.; Fan, Z. Y.; Ding, S. J.; Yu, D. M.; Du, Y. P. Fabrication of MoS_2 Nanosheet@TiO_2 Nanotube Hybrid Nanostructures for Lithium Storage. *Nanoscale* **2014**, *6*, 5245−5250.
(18) Lau, V. W.; Masters, A. F.; Bond, A. M.; Maschmeyer, T. Ionic-Liquid-Mediated Active-Site Control of MoS_2 for the Electrocatalytic Hydrogen Evolution Reaction. *Chem. - Eur. J.* **2012**, *18*, 8230−8239.
(19) Yan, Y.; Xia, B.; Ge, X.; Liu, Z. L.; Wang, J. Y.; Wang, X. Ultrathin MoS_2 Nanoplates with Rich Active Sites as Highly Efficient Catalyst for Hydrogen Evolution. *ACS Appl. Mater. Interfaces* **2013**, *5*, 12794−12798.
(20) Li, Y.; Wang, H.; Xie, L.; Liang, Y. Y.; Hong, G. S.; Dai, H. J. MoS_2 Nanoparticles Grown on Graphene: An Advanced Catalyst for the Hydrogen Evolution Reaction. *J. Am. Chem. Soc.* **2011**, *133*, 7296−7299.
(21) Meng, C. H.; Liu, Z. Y.; Zhang, T. R.; Zhai, J. Layered MoS_2 Nanoparticles on TiO_2 Nanotubes by a Photocatalytic Strategy for Use as High-Performance Electrocatalysts in Hydrogen Evolution Reactions. *Green Chem.* **2015**, *17*, 2764−2768.
(22) Czaja, W.; Krystynowicz, A.; Bielecki, S.; Brown, R. M. Microbial Cellulose - the Natural Power to Heal Wounds. *Biomaterials* **2006**, *27*, 145−151.
(23) Wang, B.; Li, X.; Luo, B.; Yang, J. X.; Wang, X. J.; Song, Q.; Chen, S. Y.; Zhi, L. J. Pyrolyzed Bacterial Cellulose: A Versatile Support for Lithium Ion Battery Anode Materials. *Small* **2013**, *9*, 2399−2404.
(24) Chen, C. T.; Huang, Y.; Zhu, C. L.; Nie, Y.; Yang, J. Z.; Sun, D. P. Synthesis and Characterization of Hydroxypropyl Cellulose from Bacterial Cellulose. *Chin. J. Polym. Sci.* **2014**, *32*, 439−448.
(25) Li, S.; Huang, D.; Yang, J.; Zhang, B. Y.; Zhang, X. F.; Yang, G.; Wang, M. K.; Shen, Y. Freestanding Bacterial Cellulose-Polypyrrole Nanofibres Paper Electrodes for Advanced Energy Storage Devices. *Nano Energy* **2014**, *9*, 309−317.
(26) Chen, L.; Huang, Z.; Liang, H.; Gao, H. L.; Yu, S. H. Three-Dimensional Heteroatom-Doped Carbon Nanofiber Networks Derived from Bacterial Cellulose for Supercapacitors. *Adv. Funct. Mater.* **2014**, *24*, 5104−5111.
(27) Gadim, T.; Figueiredo, A.; Rosero-Navarro, N.; Viela, C.; Gamelas, J.; Barros-Timmons, A.; Pascoal, N.; Silvestre, A.; Freire, C.; Figueiredo, F. Nanostructured Bacterial Cellulose-Poly(4-styrene sulfonic acid) Composite Membranes with High Storage Modulus and Protonic Conductivity. *ACS Appl. Mater. Interfaces* **2014**, *6*, 7864−7875.
(28) Huang, X.; Zhao, Y.; Ao, Z.; Wang, G. X. Micelle-Template Synthesis of Nitrogen-Doped Mesoporous Graphene as an Efficient Metal-Free Electrocatalyst for Hydrogen Production. *Sci. Rep.* **2014**, *4*, 7557.
(29) Liang, H. W.; Wu, Z. Y.; Chen, L. F.; Li, C.; Yu, S. H. Bacterial Cellulose Derived Nitrogen-Doped Carbon Nanofiber Aerogel: An Efficient Metal-Free Oxygen Reduction Electrocatalyst for Zinc-Air Battery. *Nano Energy* **2015**, *11*, 366−376.
(30) Hu, W.; Chen, S.; Yang, Z.; Liu, L. T.; Wang, H. P. Flexible Electrically Conductive Nanocomposite Membrane Based on Bacterial Cellulose and Polyaniline. *J. Phys. Chem. B* **2011**, *115*, 8453−8457.
(31) Long, C.; Qi, D.; Wei, T.; Yan, J.; Jiang, L. L.; Fan, Z. J. Nitrogen-Doped Carbon Networks for High Energy Density Supercapacitors Derived from Polyaniline Coated Bacterial Cellulose. *Adv. Funct. Mater.* **2014**, *24*, 3953−3961.
(32) Zhang, L. J.; Wan, M. X. Self-Assembly of Polyaniline - From Nanotubes to Hollow Microspheres. *Adv. Funct. Mater.* **2003**, *13*, 815−820.
(33) Ding, S.; Zhang, D.; Chen, J. S.; Lou, X. W. Facile Synthesis of Hierarchical MoS_2 Microspheres Composed of Few-Layered Nanosheets and Their Lithium Storage Properties. *Nanoscale* **2012**, *4*, 95−98.
(34) Huang, Y. P.; Miao, Y. E.; Zhang, L. S.; Tjiu, W. W.; Pan, J. S.; Liu, T. X. Synthesis of Few-Layered MoS_2 Nanosheet-Coated Electrospun SnO_2 Nanotube Heterostructures for Enhanced Hydrogen Evolution Reaction. *Nanoscale* **2014**, *6*, 10673−10679.
(35) Wang, D. Z.; Pan, Z.; Wu, Z. Z.; Wang, Z. P.; Liu, Z. H. Hydrothermal Synthesis of MoS_2 Nanoflowers as Highly Efficient Hydrogen Evolution Reaction Catalysts. *J. Power Sources* **2014**, *264*, 229−234.
(36) Xie, J.; Zhang, H.; Li, S.; Wang, R. X.; Sun, X.; Zhou, M.; Zhou, J. F.; Lou, X. W.; Xie, Y. Defect-Rich MoS_2 Ultrathin Nanosheets with Additional Active Edge Sites for Enhanced Electrocatalytic Hydrogen Evolution. *Adv. Mater.* **2013**, *25*, 5807−5813.
(37) Chang, Y. H.; Revannath, D.; Nikam; Lin, C. T.; Huang, J. K.; Tseng, C. C.; Hsu, C. L.; Cheng, C. C.; Su, C. Y.; Li, L. J.; Chua, D. Enhanced Electrocatalytic Activity of MoS_x on TCNQ-Treated Electrode for Hydrogen Evolution Reaction. *ACS Appl. Mater. Interfaces* **2014**, *6*, 17679−17685.
(38) Guo, X.; Cao, G.; Ding, F.; Li, X. Y.; Zhen, S. Y.; Xue, Y. F.; Yan, Y. M.; Liu, T.; Sun, K. N. A Bulky and Flexible Electrocatalyst for Efficient Hydrogen Evolution Based on the Growth of MoS_2 Nanoparticles on Carbon Nanofiberfoam. *J. Mater. Chem. A* **2015**, *3*, 5041−5046.
(39) Fei, H. L.; Yang, Y.; Peng, Z. W.; Ruan, G. D.; Zhong, Q. F.; Li, L.; Errol, L. G.; James, M. T. Cobalt Nanoparticles Embedded in Nitrogen-Doped Carbon for the Hydrogen Evolution Reaction. *ACS Appl. Mater. Interfaces* **2015**, *7*, 8083−8087.
(40) Liu, Q.; Pu, Z. H.; Asiri, A. M.; Sun, X. P. Nitrogen-Doped Carbon Nanotube Supported Iron Phosphide Nanocomposites for Highly Active Electrocatalysis of the Hydrogen Evolution Reaction. *Electrochim. Acta* **2014**, *149*, 324−329.

DOI: 10.1021/acsami.5b06274
ACS Appl. Mater. Interfaces 2016, 8, 3558−3566

(41) Zhou, W.; Zhou, K.; Hou, D.; Liu, X. J.; Li, G. Q.; Sang, Y. H.; Liu, H.; Li, L. G.; Chen, S. M. Three-Dimensional Hierarchical Frameworks Based on MoS_2 Nanosheets Self-Assembled on Graphene Oxide for Efficient Electrocatalytic Hydrogen Evolution. *ACS Appl. Mater. Interfaces* **2014**, *6*, 21534−21540.
(42) Liu, N.; Yang, L.; Wang, S.; Zhong, Z. W.; He, S.; Yang, X. Y.; Gao, Q. S.; Tang, Y. Ultrathin MoS_2 Nanosheets Growing within an In-Situ-Formed Template as Efficient Electrocatalysts for Hydrogen Evolution. *J. Power Sources* **2015**, *275*, 588−594.
(43) Ji, S. S.; Yang, Z.; Zhang, C.; Liu, Z. Y.; Tjiu, W. W.; Phang, I. Y.; Zhang, Z.; Pan, J. S.; Liu, T. X. Exfoliated MoS_2 Nanosheets as Efficient Catalysts for Electrochemical Hydrogen Evolution. *Electrochim. Acta* **2013**, *109*, 269−275.
(44) Li, F.; Zhang, L.; Li, J.; Lin, X. Q.; Li, X. Z.; Fang, Y. Y.; Huang, J. W.; Li, W. Z.; Tian, M.; Jin, J.; Li, R. Synthesis of Cu-MoS_2/rGO Hybrid as Non-Noble Metal Electrocatalysts for the Hydrogen Evolution Reaction. *J. Power Sources* **2015**, *292*, 15−22.
(45) Gong, C.; Huang, C.; Miller, J.; Cheng, L. X.; Hao, Y. F.; Cobden, D.; Kim, J. Y.; Ruoff, R.; Wallace, R.; Cho, K.; Xu, X. D.; Chabal, Y. Metal Contacts on Physical Vapor Deposited Monolayer MoS. *ACS Nano* **2013**, *7*, 11350−11357.

DOI: 10.1021/acsami.5b06274
ACS Appl. Mater. Interfaces 2016, 8, 3558−3566